Stabilization of a Novel Enzyme·Substrate Intermediate in the Y206F Mutant of *Candida albicans* EBP1: Evidence for Acid Catalysis†

James Buckman and Susan M. Miller*

Department of Pharmaceutical Chemistry, University of California School of Pharmacy, San Francisco, California 94143-0446

Received March 21, 2000; Revised Manuscript Received June 16, 2000

ABSTRACT: EBP1-catalyzed reduction of α,β-unsaturated ketones and aldehydes is proposed to proceed via transfer of hydride from the flavin to the β-position of the olefinic bond, concomitant with or followed by uptake of a proton at the α-position. Structural analysis suggests that this proton is donated from Tyr206, and, hence, a protein was constructed in which it was replaced by phenylalanine. The mutation results in a slightly less stable protein than the wild type that nevertheless retains the fundamental flavin and phenol binding properties of EBP1 characterized previously. The pH profile for binding of phenol was characterized over the pH range 6.5−9.5 and was found to be simpler than that for the wild-type enzyme. Most importantly, a pK_a of 8.7 that is perturbed to 9.4 upon binding of phenol to the wild-type enzyme is missing in the mutant, allowing assignment of this pK_a to the Y206 hydroxyl group. Additionally, the pK_a of phenol is further lowered from its value of 10.0 in solution to ≈6.4 in the active site of the mutant, as compared to 7.1 in the wild type. Together, these perturbations lead to an increase of ≈35-fold in the binding affinity of the mutant for phenol at high pH relative to the affinity of the wild-type enzyme. As expected, the mutation has little effect on the reductive half-reaction, in which a hydride equivalent is transferred from NADPH to the flavin. In contrast, the reduction of *trans*-2-hexenal by the reduced enzyme is significantly affected. The results indicate formation of a previously unobserved charge-transfer (CT) complex following formation of the Michaelis complex between substrate and reduced enzyme and preceding reduction of the substrate, which occurs at a greatly reduced rate (≥440-fold) relative to wild type. Thus, while the oxidative half-reaction with wild-type enzyme is limited by the rate of formation of the CT complex, it is the chemical step that is rate-limiting in the reaction with EBP1:Y206F, consistent with the role of this residue as a general acid.

In the preceding manuscript (*21*), we presented a detailed analysis of the kinetics and intermediates formed during the two half-reactions of the EBP1[1]-catalyzed transfer of electrons from NADPH to an α,β-unsaturated aldehyde, *trans*-2-hexenal. The results suggest that NADPH is the likely reductant of this enzyme, but the physiological electron acceptor is unknown. One of the primary goals of the study was to understand the mechanism enough to design appropriate mutants with which to trap the enzyme's physiological substrate. Thus, if an altered enzyme can be designed to bind but not reduce the substrate, it may be possible to capture, isolate, and characterize the compound.

Steady-state analysis of the mechanism for the EBP1-catalyzed reaction indicates ping-pong behavior, with NADPH binding, oxidation, and dissociation preceding binding and reaction with the electron-accepting substrate (*3*). The microscopic behavior during the second half-reaction, in which a hydride equivalent is transferred from the flavin to a variety of electron acceptors with an α,β-unsaturated ketone or aldehyde functional group, might be better understood in the context of conclusions from studies of similar systems, e.g., the acyl-CoA dehydrogenases (*22*, *23*). In these proteins, the saturated acyl-CoA substrate is oxidized by hydride transfer from the β-position of the substrate to the flavin, and a base (a glutamate residue) in the active site abstracts a proton from the α-position. Speculating that a similar strategy might be employed by EBP1 in reverse, we sought to identify an acidic residue that could donate a proton to the α-carbon during reduction of the substrate. A residue with this function should be relatively unimportant to the first half-reaction, where transfer of hydride from NADPH to the flavin generates $NADP^+$, with no requirement for proton abstraction or donation at the pyridine nucleotide ring. Mutation of such a residue might then yield an enzyme that can still be reduced by NADPH, but cannot reduce the electron-accepting substrate, thereby allowing the substrate to be trapped.

Though a crystal structure of EBP1 has not yet been solved, several structures of the well-studied homologue OYE1 are available (*4*). These include one in which the

† This work was supported in part by grants to S.M.M. from the UCSF Academic Senate and the Charles E. Culpeper Foundation. J.B. was supported in part by an American Foundation for Pharmaceutical Education Fellowship and a University of California President's Dissertation Year Fellowship.

* To whom correspondence should be addressed. Email: smiller@cgl.ucsf.edu; tel: 415-476-7155; fax: 415-476-0688.

[1] Abbreviations: EBP1, estrogen binding protein; E_{ox}, oxidized EBP1; E_{red}, reduced EBP1; NADPH, nicotinamide adenine dinucleotide phosphate, reduced form; $NADP^+$, nicotinamide adenine dinucleotide phosphate, oxidized form; HXL or hexenal, *trans*-2-hexenal; FMN, flavin mononucleotide; OYE, Old Yellow Enzyme; GC, gas chromatography; CT, charge transfer; CHES, 2-(*N*-cyclohexylamino)ethanesulfonic acid; MOPS, 3-(*N*-morpholino)propanesulfonic acid; MES, 4-morpholineethanesulfonic acid; HBA, *p*-hydroxybenzaldehyde.

10.1021/bi000653s CCC: $19.00
Published on Web 08/04/2000

flavin cofactor is oxidized, one in which it is reduced by two electrons, and one with *p*-hydroxybenzaldehyde bound in the active site of the oxidized enzyme. The positions of the active site residues are quite similar in all three structures of OYE1, and, since many are conserved in the sequence of EBP1, we used these structures as a basis to identify residues likely to act as the proton donor. Examination of the active site in these structures, especially that with a ligand bound, reveals that Tyr196, corresponding to Tyr206 in the sequence of EBP1, is oriented such that the hydroxyl group might be optimally positioned to donate a proton to the α-carbon of the substrate if it is bound in the same orientation as the phenolic ligand. Given its role as a general acid in other enzymes, e.g., tyrosine phenol-lyase (*5*) and Δ^5-3-ketosteroid isomerase (*6*), and the fact that no other acidic residues lie in the immediate vicinity of the α-carbon, the tyrosine appears to be the most likely candidate. To minimize the effects of the mutation on protein packing, while eliminating the proton donor, we have generated the Y206F mutation in EBP1. In this paper, we report effects of the mutation on the phenol binding properties and on the transient kinetics of the reductive and oxidative half-reactions. During the course of our studies, Kohli and Massey (*1*) reported results of studies of the same mutation made in OYE1. Similarities and differences in the effects of this mutation on the two proteins are discussed.

MATERIALS AND METHODS

Unless indicated otherwise, all reagents were the highest grade possible and obtained from Sigma Chemical.

Construction of the Y206F Mutant. The mutant was generated using the Chameleon Double-Stranded, Site-Directed Mutagenesis Kit (Stratagene) according to the manufacturer's protocol. A primer was designed that was complementary to the coding strand of the pET-3a vector into which the EBP1 coding sequence had previously been inserted. This primer, GGCAAGATTTAAAAACTGATC-CAAGAAACCATGAGCACC, complements nucleotides 601−646 in the EBP1 sequence, with the exception of a point substitution (underlined) that results in the encoding of a phenylalanine corresponding to position 206 in the wild-type amino acid sequence. This primer also results in the elimination of an *Mae* III restriction endonuclease site to facilitate identification of appropriate transformants. The original pET-3a construct was purified using standard techniques and used as template, and the mutagenic primer was purified with the Nucleotide Removal Kit (Qiagen) before use according to the Chameleon kit. *E. coli* XL-1 Blue competent cells (Stratagene) were transformed to select the mutagenized plasmid, and five colonies were picked from the transformants. Plasmid DNA was isolated from these cells using the Wizard Plus Miniprep DNA purification system (Promega), and digestion with *Mae* III demonstrated that four contained the appropriate insert. Plasmid DNA from one of these four was subsequently sequenced, determined to be correct, and used to transform competent *E. coli* BL21(DE3) cells to express the mutant protein.

Purification of the Mutant. The mutant was purified in the same manner as that described previously for the wild-type protein (*3*) with slight adaptations. As with wild type, the mutant protein was eluted from a *p*-hydroxybenzamide affinity resin with 100 mM Tris-HCl buffer, pH 8.3, containing 50 mM phenol. The resulting EBP1·Y206F·phenol complex was treated with KBr at a final concentration of 1.5 M in order to weaken the interaction and facilitate removal of the ligand. This solution was passed through a 500 mL column of desalting gel, Bio-Gel P-6DG (BioRad), initially equilibrated with 20 mM Tris-HCl buffer, pH 7.5, and to which a small amount (∼50 mL) of 1.5 M KBr was added at the very top of the column immediately before use. Under these conditions, the mutant protein dissociates quantitatively from the phenol as it passes through the high KBr region of the gel, and elutes ligand-free, as evidenced by the UV−visible absorption spectrum. The eluate was concentrated to a volume of ∼30 mL in a Centriprep-30 concentrator (Amicon), and all treatment that followed, including the use of the Cibacron Blue affinity purification resin (Amicon Dye Matrex), was performed as described for wild-type protein (*3*).

Scheme 1

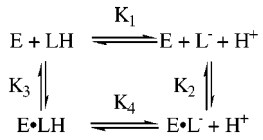

Determination of Redox Potential and Extinction Coefficient. The midpoint reduction potential and extinction coefficients at 386 and 466 nm of EBP1·Y206F were determined in the same fashion as described for wild type (*3*).

Gel Exclusion Analysis. Stock solutions of all protein samples (1 mg/mL) were prepared in either 50 mM CHES buffer, pH 9.1, containing 200 mM KCl or 50 mM MOPS buffer, pH 6.0, containing 200 mM KCl for the high and low pH conditions, respectively. Chicken egg white lysozyme (MW = 14 400), *A. niger* glucose-6-phosphate dehydrogenase (MW = 104 000), and bovine serum albumin (MW = 66 000 and 132 000 for the dimer and tetramer, respectively) were used as molecular weight standards. A 50 μL aliquot of enzyme or standard was injected onto a Superose 12 HR gel filtration column fitted to an FPLC apparatus (Amersham Pharmacia Biotech). Samples were run isocratically in the appropriate buffer after overnight equilibration of the column at a flow rate of 1 mL/min. Elution was monitored using a UV−visible detector set at 280 nm.

Phenol Binding Titrations. All titrations were performed in a buffer system consisting of 100 mM MES, 51 mM *N*-ethylmorpholine, and 51 mM diethanolamine, which maintains nearly constant ionic strength across the pH range 6.5−9.5 (*7*). Typically, a stock solution of enzyme in 1 mM potassium phosphate buffer, pH 7.5, was diluted 10-fold into the buffer system above, which had been adjusted to the appropriate pH with either HCl or KOH. Stock solutions of phenol were dissolved in titration buffer. Spectra were recorded using a Shimadzu UV-2101PC double-beam absorbance spectrophotometer, and resulting data were analyzed using SPECFIT (Spectrum Software Associates, Chapel Hill, NC), a program that employs a singular value decomposition routine, global least-squares fitting, and factor analysis of the entire set of spectral data to yield values for kinetic or equilibrium binding constants for a specified model.

The pH dependence of the apparent dissociation constants obtained using SPECFIT was evaluated for the involvement

Scheme 2

$$E_{ox} + NADPH \underset{k_2}{\overset{k_1}{\rightleftharpoons}} E_{ox}\bullet NADPH \underset{k_4}{\overset{k_3}{\rightleftharpoons}} E_{ox}\bullet NADPH^{*} \underset{k_6}{\overset{k_5}{\rightleftharpoons}}$$

$$E_{red}\bullet NADP^{+} \underset{k_8}{\overset{k_7}{\rightleftharpoons}} E_{red} + NADP^{+}$$

Scheme 3

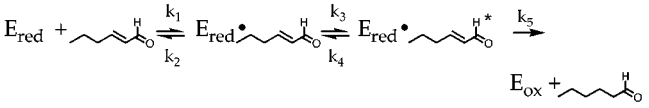

of one or two titratable groups in the enzyme and ligand combination (*8*). Scheme 1 shows the relevant equilibria involving a single titratable group, and eq 1 shows the analytical solution for $K_{d(app)}$ for this model.

$$-\log K_{d(app)} = \log\left(1 + \frac{K_4}{[H^+]}\right) - \log\left(1 + \frac{K_1}{[H^+]}\right) - \log K_3 \quad (1)$$

For the system studied here, K_1 is the acid dissociation constant for phenol in solution, and K_4 is that value for phenol bound to the protein.

Synthesis of β-[4(R)-²H]NADPH. Isotopically labeled NADPH was prepared as described in the preceding paper (*21*), and the experiments featured here were performed using the same material, either directly before or after those detailed in the work with wild type (*3*).

Stopped-Flow Experiments. All rapid reaction studies were conducted using a HiTech SF-61DX2 instrument (Hi-Tech Ltd., Salisbury, U.K.), in the same fashion as that described in the preceding paper for the wild-type enzyme (*21*).

Data Presentation and Curve Fitting. Both single-wavelength and diode array kinetic data were analyzed and rendered as described in the preceding paper (*21*).

Kinetic Simulations. Single-wavelength stopped-flow data were exported from the KinetAsyst software as text files, and a deadtime of 1.54 ms, experimentally determined for this instrument according to the manufaturer's protocol, was added to all time points.

As described below, the reductive half-reaction with the mutant protein is quite similar to that with wild type. Thus, the model used to simulate the wild-type data, Scheme 2, was also used to simulate the data collected with the mutant. Estimates and constraints for the values of the intrinsic constants for simulating this reaction in the forward direction were assembled from the values of the observed rate constants and the fluorescence quench data.

The concentration dependence of k_{1obs} for the oxidative half-reaction is best fit by eq 2:

$$k_{1obs} = \frac{k_3 \times [HXL]}{[HXL] + K_d} + k_4 \quad (2)$$

which is characteristic of the behavior of a fully reversible two-step equilibrium process (first two steps in Scheme 3) in which the signal arises from the final species (E_{red}·HXL*) and $K_d = k_2/k_1$ (*9*).

The concentration dependence of k_{2obs} is best fit by eq 3, which again derives from a two-step equilibrium reaction, where the second step is effectively irreversible.

$$k_{2obs} = \frac{k_{max} \times [HXL]}{[HXL] + K_{d(app)}} \quad (3)$$

However, as will be described below, the process observed in this transient follows that characterized by k_{1obs}. Thus, the appropriate model to describe the overall reaction involves three steps as shown in Scheme 3. Expressions for $K_{d(app)}$ and k_{max} in eq 3 therefore include terms for all three steps, and are given by eqs 4 and 5, respectively.

$$K_{d(app)} = \frac{[E_{red}][HXL]}{[E_{red}\bullet HXL] + [E_{red}\bullet HXL^*]} = \frac{(k_2/k_1)(k_4)}{k_3 + k_4} \quad (4)$$

$$k_{max} = k_5 \times \left(\frac{k_3}{k_3 + k_4}\right) \quad (5)$$

Although eq 2 adequately describes the behavior of k_{1obs}, it is derived with the assumption that $k_2 \gg k_3$. An equally valid fit of the data can be obtained using an alternative form of eq 2 that includes all four rate constants (k_1 through k_4) and makes no assumptions as to their relative values. However, a unique solution for all four constants cannot be obtained by simple analysis of the concentration dependence. To examine this further, data traces for the oxidative half-reaction collected at 650 nm were simulated using a model constructed in KINSIM based on the mechanism depicted in Scheme 3. Initial estimates for the microscopic rate constants used in the simulations were obtained from the analyses of the observed rate constants using eqs 2−5. Values for the extinction coefficient of the CT species at 650 nm, ϵ_{CT}, used in each round of simulation were calculated using the values of k_4 and k_3 for that iteration in eq 6:

$$\epsilon_{CT} = \epsilon_{obs}\frac{[E_{red}\bullet HXL] + [E_{red}\bullet HXL^*]}{[E_{red}\bullet HXL^*]} = \epsilon_{obs}(k_4/k_3 + 1) \quad (6)$$

where ϵ_{obs} is the observed extinction coefficient calculated from the maximal absorbance occurring at this wavelength using a saturating substrate concentration, and k_4/k_3 describes the internal equilibrium between the Michaelis and CT complexes in Scheme 3. The extinction coefficients used in simulating data collected at 466 nm for the oxidative half-reaction in the wild-type enzyme were determined as follows. That for the reduced enzyme·hexenal Michaelis complex was assumed to be equivalent to that for free reduced enzyme, determined in reductive titrations of the enzyme with sodium dithionite (not shown). The value for the charge-transfer complex was calculated from the spectrum of the fully formed CT complex of the mutant (see above) and assumed to be the same as it is in that protein. Finally, the extinction coefficient used for the oxidized enzyme was that reported previously (*3*).

Reaction Product Analysis. Reactions were incubated for 2 h in 100 mM potassium phosphate buffer, pH 7.0, using a final concentration of 1 μM wild type or 3 μM mutant EBP1, and 1 mM concentrations of both NADPH and the oxidizing substrate. The mixtures were then extracted twice with 1 mL

of methylene chloride, and the organic phases were combined and dried over anhydrous sodium sulfate. Solvent was evaporated under a stream of argon, until ~30 μL remained. Ten microliters of each sample prepared in this way was injected into a Hewlett-Packard 5890 GC system fitted with a 30 m DB-1 capillary column, 0.25 mm internal diameter. The injector temperature was maintained at 200 °C, and the carrier gas was helium at a head pressure of 16 psi. The standard procedure involved injection onto the column held at 60 °C until elution of the compound of interest. The temperature was then increased to 300 °C and held there for 30 min between runs. Product retention times for the reaction with hexenal were compared with those of hexenal, hexanal, and 2-hexen-1-ol. For the reaction with cyclohexenone, products were compared with cyclohexenone, cyclohexanone, and 2-cyclohexen-1-ol. Retention of the sample extracted from the reaction with cinnamaldehyde was compared with that of cinnamaldehyde and 3-phenylpropionaldehyde.

RESULTS

General Properties of the Mutant. The UV−visible absorption spectra of the mutant and wild-type proteins are nearly identical, suggesting that the mutation is not grossly destabilizing, and that the electronic environment of the FMN cofactor is reasonably maintained. Qualitatively, however, the structural integrity of the protein does seem to be somewhat compromised, especially in comparing the behavior of the mutant during physical manipulation with that of wild type. For instance, the "durability" of the proteins during ligand titration was very different, where pipetting and tipping of solutions of the proteins is necessary to achieve good mixing. The mutant required much more delicate handling to prevent precipitation. This problem was exacerbated by higher temperatures and/or pH.

In initial attempts to isolate the mutant enzyme, a small amount of long-wavelength absorbance was consistently present in the absorption spectrum that remained even after the extensive purification regime described above. This behavior was previously reported for the wild-type protein (*3*), where dialysis was found to eliminate the absorbance band. This absorbance phenomenon has a long history in the study of the EBP1 homologue OYE (*10*), and has also been shown for wild-type EBP1 to be associated with the electronic interaction between various ligands and the flavin cofactor. Thus, we suspected that this persistent feature of the mutant spectrum is due to the presence of a ligand. The success of the purification protocol, both in the initial binding to the affinity column and for elution with phenol, indicates that the mutant binds this compound tightly (see below). However, the vigorous efforts to remove the phenol, and a difference in the position of the CT absorbance band with phenol vs that in the final purified enzyme suggested that the remaining ligand is not phenol. This, in fact, seems to be the case, since the protein can now be reproducibly isolated without this absorbance band when effort is made to avoid exposure to plastics (e.g., syringes, filters, etc.) that have not been thoroughly rinsed before use. Thus, it appears that a contaminant is present in the unwashed plastics, such as a remnant of the synthetic process, that binds to the protein. It has previously been suggested that there are substances associated with plastic that mimic estrogens in biological systems (*11*). Given the binding characteristics of both the wild type and this mutant estrogen binding protein, this seems a likely possibility.

A value of −233 mV was determined for the midpoint potential of the $E_{ox} + 2e^- \rightarrow E_{red}$ couple (data not shown), ≈13 mV more positive than that for wild type. The small magnitude of the perturbation is consistent with the prediction that the tyrosyl hydroxyl group lies in the vicinity of the active site, but is not in direct contact with the flavin. The direction of the perturbation presages the significant impact the mutation makes on other functional aspects.

Oligomerization Analysis. In light of the structural effects of the mutation implied by the lower stability of the mutant, we investigated the oligomerization state as compared to the wild-type protein. The literature has been somewhat confusing in this regard, with different reports of wild-type EBP1 existing solely as monomer or dimer (*12, 13*). Preliminary results we obtained with the wild-type protein were consistent with a monomeric state in the presence of varied salt concentrations, with or without 17β-estradiol (unpublished observations). We have subsequently conducted a gel filtration assay in which both proteins were analyzed under mildly acidic (pH 6) and basic (pH 9) conditions. The elution volume was identical for both the wild type and mutant under all conditions and indicates a MW of 50 000, in good agreement with the calculated MW of 46 073 for the protein monomer (data not shown). Thus, the mutation has no impact on the oligomerization of the protein under the conditions studied.

Phenol Binding. A substantial effect of the mutation on phenol binding was apparent during the first purification of the protein. Elution of the mutant from the *p*-hydroxybenzamide affinity column with phenol gave a much darker, greener eluate than that typically observed with wild-type enzyme. The underlying basis of this is a 30 nm red shift in the long-wavelength absorbance band of the phenol complex of mutant relative to that of wild-type enzyme (Figure 1A, inset). The long-wavelength band is attributed to a charge-transfer (CT) interaction, where excitation by light of the appropriate energy leads to the promotion of an electron from a molecular orbital in the donor molecule (phenoxide) to one in the acceptor (oxidized FMN) (*2, 3, 14*). Thus, the shift of the CT absorbance band relative to that in the wild-type complex reflects a change in the relative energies of the orbitals involved. The fact that it is red-shifted implies that the electron transfer is more facile (requires less energy) than it is with wild-type enzyme, and is consistent with the observed increase in the reduction potential of the mutant.

Examination of the effect of pH on the binding affinity of phenol to wild-type enzyme previously revealed perturbations in the pK_a values for both phenol and a residue on the enzyme upon formation of the complex (*3*). The pK_a of phenol decreases from 10.0 in solution to 7.1 in the wild-type complex, while the pK_a of the enzyme residue increases from 8.7 to 9.4. With its expected position over the substrate/phenol binding site and its predicted role as an acid catalyst, Y206 seems to be a good candidate for the residue with pK_a 8.7. As shown in Figure 1B, the affinity of the mutant for phenol again increases with increasing pH, as with wild type, but the data are well fit with a model (Scheme 1) involving perturbation of only one pK_a, a decrease of the value for phenol from 10.0 in solution to ~6.4 in the enzyme complex. Thus, it appears that the Y206 hydroxyl group is indeed the

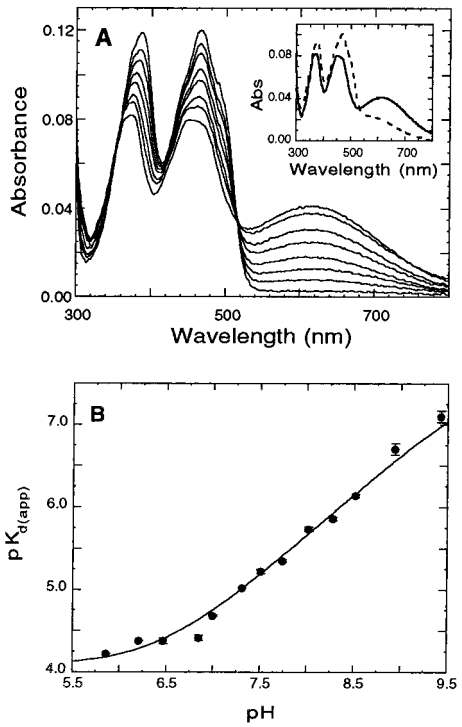

FIGURE 1: Titration of EBP1·Y206F with phenol. (A) Y206F (11 μM) was titrated with phenol at pH 7.0 in the buffer system described in the text. Spectra were collected after addition of phenol to a final concentration of 0, 4.2, 8.4, 16.7, 27.0, 47.3, 86.6, and 229.3 μM and are dilution-corrected. Inset: Spectra of saturated phenol complexes of mutant (solid line) and wild-type (dashed line) enzymes at pH 7.0, dilution-corrected and normalized for difference in enzyme concentration. (B) Dissociation constants were determined as described in the text. The solid line represents a fit to the data using eq 1, and yields the following values for the equilibrium constants shown in Scheme 1: $K_3 = (8 \pm 2) \times 10^{-5}$ M, $K_4 = (3.7 \pm 0.9) \times 10^{-7}$ M. The acid dissociation constant for phenol in solution was set at that reported in the literature (*15*), $K_1 = 1.0 \times 10^{-10}$, and by completion of the thermodynamic cycle (Scheme 1), $K_2 = 2 \times 10^{-8}$ M.

titratable residue of pK_a 8.7 in the wild-type enzyme. At 1.4 units lower than the solution pK_a for a tyrosine hydroxyl (*15*), this value indicates a 25-fold increase in the acidity of this residue in the active site, consistent with its predicted role as a proton donor in the oxidative half-reaction. In addition to the loss of this enzymic pK_a, the mutation leads to a further lowering of the pK_a for bound phenol by 0.7 log unit, consistent with removal of the electron density of the Y206 hydroxyl group in the vicinity of the electron-rich phenoxide ring. At high pH, deprotonation of the enzyme residue in the wild type leads to a decrease in the affinity for phenoxide, consistent with a negative electrostatic interaction between the tyrosyl anion and the adjacent phenoxide ligand. The absence of this effect in the mutant leads to a substantial increase in the stabilizing interactions between the enzyme and phenoxide, resulting in an increase of approximately 35-fold in the binding affinity of the mutant for phenoxide at high pH.

Reductive Half-Reaction with NADPH. Spectral changes obtained in the diode array mode of the stopped flow during reduction of Y206F with NADPH indicate that the reaction proceeds much as it does with wild type (data not shown). The higher resolution of the instrument in the photomultiplier mode was again required to observe the first phase of this

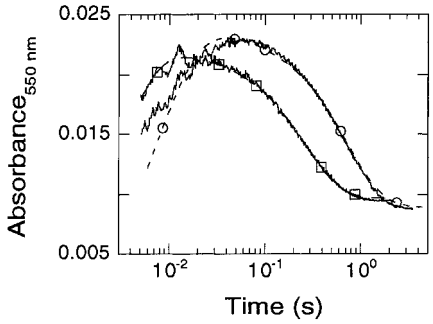

FIGURE 2: Rapid mixing of EBP1·Y206F with NADPH or β-[4(R)-^{2}H]-NADPH in the stopped flow. Semilogarithmic plot of UV−visible absorbance data collected at 550 nm in the single-wavelength mode after mixing of 10.3 μM enzyme and 100 μM NADPH or β-[4(R)-^{2}H]-NADPH (final concentrations). Simulated data (dashed line) using the constants given in Table 1 are overlaid onto the raw data (solid line) using unlabeled (□) and deuterated (○) NADPH, respectively.

Table 1: Microscopic Rate Constants for the Reduction of EBP1·Y206F with NADPH and β-[4(R)-^{2}H]-NADPH

constants	with NADPH[a]	with β-[4(R)-^{2}H]-NADPH[b]
k_1	2×10^7 M^{-1} s^{-1}	2×10^7 M^{-1} s^{-1}
k_2	1 s^{-1}	1 s^{-1}
k_3	250 s^{-1}	95 s^{-1}
k_4	125 s^{-1}	37 s^{-1}
k_5	3.1 s^{-1}	1.2 s^{-1}
k_6	21 s^{-1}	6 s^{-1}
$k_{7/k8}$	8×10^{-5} M	8×10^{-5} M

[a] Determined from overlay of raw and simulated data for reactions monitored at 405, 487, and 550 nm (see Figure 2). [b] Determined from overlay of raw and simulated data for reactions monitored at 550 nm.

process (Figure 2). The reaction is characterized by the rapid development of a long-wavelength-absorbing (CT) species followed by a much slower loss of absorbance in the flavin and CT absorption bands, consistent with transfer of hydride from NADPH to the flavin. Modeling the reaction as an irreversible biphasic process yields values for the observed rate constants of 249 ± 6 and 3.84 ± 0.03 s^{-1}. As in the wild-type reaction, the rate constants associated with both phases are independent of the NADPH concentration (data not shown). This indicates the presence of an equilibrium binding step preceding the transient leading to formation of the CT absorbance that is saturated and complete within the deadtime, even at the lowest concentration of NADPH used. To monitor this process, we followed the loss of fluorescence of NAPDH upon binding to the mutant as we had with wild-type EBP1. The rate constant for association of NADPH and the mutant was determined to be $(2.0 \pm 0.2) \times 10^7$ M^{-1} s^{-1} from the dependence of the observed rate on protein concentration (data not shown), identical within error to the value determined for NADPH and wild type (Buckman and Miller, *21*). Analysis of the transient kinetic data for the mutant was carried out in the same fashion as described for the wild-type enzyme. The data are consistent with the same model used to describe the reductive half-reaction with wild type (Scheme 2), and the microscopic rate constants, determined by iterative simulation and fits of data sets obtained from the variety of experimental techniques, are summarized in Table 1. Comparison of the constants in Table 1 with those for the wild type (see *21*) indicates that the mutation has little effect on the reductive half-reaction, in accord with the hypothesis presented in the introduction. The

most significant differences are slight increases in the equilibrium constant for formation of the charge-transfer complex [$k_3/k_4 = K_{CT}$(WT) = 1.5 vs K_{CT}(Y206F) = 2], and in the internal reduction equilibrium that favors more reduction of the flavin in the mutant than in the wild type [$k_5/k_6 = K_{red}$(WT) = 0.1 vs K_{red}(Y206F) = 0.15]. This variance between the mutant and wild type is consistent with the more positive midpoint potential for FMN on the mutant, although the 13 mV difference between the measured potentials of the free proteins might have suggested a more substantial effect on K_{red}. The small effect observed may reflect a smaller difference between the potential of the flavin cofactor on the two proteins when substrate is bound. Another possible explanation for this discrepancy is described below.

Isotope Effects with β-[4(R)-²H]-NADPH. The half-reaction with this enzyme was further probed using the same stereoisomer of deuterated NADPH that transfers deuterium to the flavin in the wild-type reaction. Again the results paralleled those obtained for wild-type EBP1, and a kinetic isotope effect was observed on both apparent phases when the reaction is modeled as an irreversible biphasic process, or simulated as the multi-equilibrium reaction of Scheme 2. As expected, both observed rate constants are concentration independent (data not shown). Simulations of the data traces were performed, and a typical trace is compared in Figure 2 with one from the NADPH reaction. The rate constants that result from these simulations are presented in Table 1.

Oxidative Half-Reaction with trans-2-Hexenal. If the hypothesis that Tyr206 functions as a general acid catalyst in the second half-reaction is correct, it follows that mutation of this residue to one incapable of proton donation should cripple the enzyme's ability to reduce the electron acceptor. Comparison of the results in Figure 3 with Figure 7 in reference (*21*) shows that the behavior of the wild-type and mutant proteins is quite different. Whereas wild-type EBP1 is reoxidized by hexenal in a single phase, the Y206F protein is reoxidized biphasically, with the rapid formation of a long-wavelength-absorbing intermediate followed by a much slower appearance of the main flavin absorbance. The spectral characteristics of the intermediate are similar to those observed in complexes of reduced acyl-CoA dehydrogenases with enoyl-CoA compounds (*16*), strongly suggesting that the intermediate is a charge-transfer complex between the reduced flavin cofactor and the oxidized enal substrate. Thus, the oxidative half-reaction appears to be analogous to the reductive half-reaction with formation of a CT complex prior to the actual electron transfer between the flavin and the substrate. To obtain better kinetic resolution, the reaction was monitored at 650 nm using the photomultiplier mode of the stopped-flow spectrophotometer. The insets to Figure 3 depict the dependence on hexenal concentration of the observed rate constants for formation (top) and decay (bottom) of the CT species. In both cases, a saturating dependence on hexenal is observed. The data for k_{1obs} (Figure 3, top inset) are best fit by a hyperbola with a nonzero *y*-intercept (eq 2), which is characteristic of the behavior of a fully reversible two-step equilibrium process (*9*). This is exactly analogous to the reductive half-reaction, where initial formation of an undetectable Michaelis complex is followed by formation of a CT complex before electron transfer. However, in this case, the dissociation constant ($K_d = k_2/k_1$)

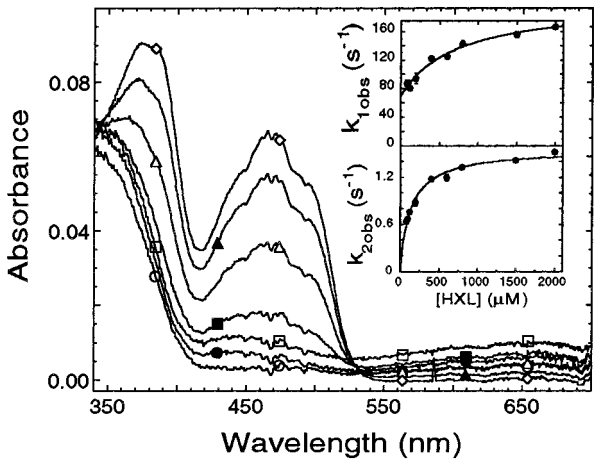

FIGURE 3: Rapid mixing of EBP1·Y206F with *trans*-2-hexenal in the stopped flow. Enzyme was reduced anaerobically with an NADPH-generating system, as described, and spectra were collected in the diode array mode after mixing with hexenal (final concentrations: 8.8 μM Y206F, 220 μM HXL). Selected spectra taken at 5 (○), 15 (●), 35 (□), 370 (■), 1320 (△), 3220 (▲), and 9500 (◇) ms are shown. Note that the maximal amplitude of the charge-transfer band in this experiment is only ~33% of that observed at saturating concentrations (≥1.5 mM), but it was chosen to illustrate CT development, which occurs too quickly to resolve well in the diode array mode. Top inset: Observed rate constant for CT formation, k_{1obs}, at varied concentrations of hexenal. The curve is a least-squares fit to eq 2 and yields values of 130 ± 10 and 68 ± 6 s^{-1} for k_3 and k_4, respectively, and a value for K_d of 700 ± 250 μM. Bottom inset: Observed rate constant for CT decay, k_{2obs}, at varied concentrations of hexenal. The curve is a least-squares fit to eq 3, and yields an apparent K_d of 130 ± 12 μM, and a maximal k_{obs} of 1.55 ± 0.03 s^{-1}.

for hexenal is weak enough to observe the concentration dependence. The rate constant for decay of the CT, k_{2obs}, also shows a saturating dependence on hexenal concentration (Figure 3, bottom inset). However, in this case, the data are best fit to a simple hyperbolic expression with a value of zero for the *y*-intercept (eq 3) indicating that the electron transfer step is irreversible. The observation of a saturating concentration dependence for both transients, where the spectral changes clearly show that one step follows the other, is consistent with the mechanism shown in Scheme 3. In addition, the sensitivity of the second phase to substrate concentration indicates that a rapid equilibration of the CT species with the free enzyme and Michaelis complex takes place before hydride transfer; that is, $k_5 \ll$ all other constants. In this case, the concentration at which k_{2obs} is half-maximal represents an apparent dissociation constant that reflects both equilibria governing CT formation (eq 4). Likewise, the maximal value for k_{2obs} reflects the microscopic rate constant for hydride transfer and the fraction of the enzyme present in the CT complex at equilibrium (eq 5). As mentioned under Materials and Methods, the validity of the values obtained from the analysis of the k_{1obs} data using eq 2 depends on the assumption that $k_2 \gg k_3$ in Scheme 3. Although an expression can be derived without this assumption (*9*) (eq 7)

$$k_{1obs} = \frac{k_1[\mathrm{HXL}](k_3 + k_4) + k_2k_4}{k_1[\mathrm{HXL}] + k_2 + k_3} \qquad (7)$$

a unique solution for all four rate constants cannot be obtained directly, since this type of curve can be adequately

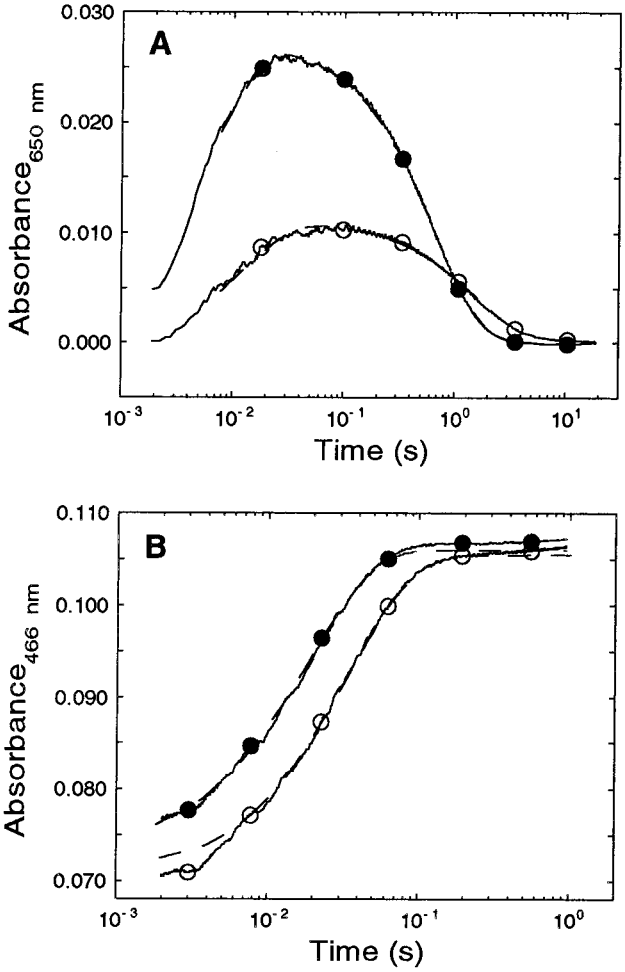

FIGURE 4: Simulation of data from rapid reaction of mutant and wild-type enzymes with *trans*-2-hexenal. (A) Data traces shown were collected at 650 nm in the photomultiplier mode of a stopped-flow instrument after rapid mixing of 600 μM (○) and 2.00 mM (●) hexenal with 8.8 μM EBP1·Y206F (final concentrations) reduced anaerobically with an NADPH-generating system (solid line). Simulated data, overlaid for comparison (dashed lines), were generated using the model of Scheme 3, values for rate constants presented in Table 2, and an extinction coefficient of 4660 M^{-1} cm^{-1} for the E_{red}·hexenal* CT complex, with the assumption that this is the only absorbing species at 650 nm. (B) Data traces collected at 466 nm in the photomultiplier mode of the stopped-flow instrument after rapid mixing of 100 μM (○) and 1.80 mM (●) hexenal with 9.5 μM wild-type EBP1, reduced in the same way as in (A). Simulated data are overlaid for comparison (dashed lines), as in (A), with the following extinction coefficients for each species, determined as described under Materials and Methods: $\epsilon_{466}(E_{red}) = 600$, $\epsilon_{466}(E_{red}{\cdot}HXL) = 600$, $\epsilon_{466}(E_{red}{\cdot}HXL^*) = 6240$, and $\epsilon_{466}(E_{ox}) = 10\,750$ M^{-1} cm^{-1}.

defined by three parameters. Thus, estimates for all of the microscopic constants were obtained from simulations of data traces collected at 650 nm using low, intermediate, and high substrate concentrations. The simulations were carried out using varied combinations of rate constants and the implicit extinction coefficient for the CT species (as described under Materials and Methods) until a set of values was obtained that represented all three data sets reasonably well. Figure 4A depicts a representative data trace overlaid with simulated data using the rate constants given in Table 2 and an extinction coefficient for the CT complex of 4660 M^{-1} cm^{-1}. The values in Table 2 are averages of those found to reproduce each individual data trace, and the apparent K_d for hexenal, calculated with eq 4, is 108 μM, in good agreement with the value of 130 μM obtained from the hyperbolic fit for k_{2obs} (Figure 3, bottom inset). To verify the values, simulated data traces were generated for all concentrations of hexenal used to obtain values for k_{1obs} that match the experimental values quite well (Figure 3, top inset). Comparison of the values for k_2, k_3, and k_4 in Table 2 with the values obtained by the fit of the data to eq 2 indicates that the original assumption that $k_2 > k_3$ appears to be valid for this reaction.

Table 2: Microscopic Rate Constants for the Oxidation of EBP1 with *trans*-2-Hexenal

constants	Y206F[a]	wild type[b]
k_1	2.9×10^6 M^{-1} s^{-1}	2.9×10^6 M^{-1} s^{-1}
k_2	1050 s^{-1}	300 s^{-1}
k_3	127 s^{-1}	60 s^{-1}
k_4	54 s^{-1}	$\leq$40 s^{-1}
k_5	2.27 s^{-1}	$\geq$970 s^{-1}

[a] Determined from overlay of raw and simulated data for reactions monitored at 650 nm (see Figure 4A). [b] Determined from overlay of raw and simulated data for reactions monitored at 466 nm (see Figure 4B).

With this insight into the mechanism of the oxidative half-reaction, we can now revisit the results for the wild-type enzyme, where no CT intermediate is detected (Buckman and Miller, *21*). Although the mechanisms may differ for mutant and wild type, the simplest explanation for the disparity is that the mechanism is the same, but the values of the intrinsic rate constants differ. The observation of a monophasic reoxidation of the wild-type enzyme with a hyperbolic dependence of k_{obs} on substrate is consistent with the mechanism of Scheme 3, where CT formation (k_3) is rate-limiting. That is, once the CT intermediate is formed in the wild type, hydride transfer to the substrate is much faster ($k_5 \gg k_3$), such that any accumulation of CT is below the limit of detection. Moreover, the fact that k_{obs} extrapolates to the origin in the absence of substrate implies that the value of the rate constant for reoxidation, k_5, must also be much greater than that for the formation of the Michaelis complex from the CT complex ($k_5 \gg k_4$), so that CT formation is effectively irreversible.

To obtain estimates for the microscopic rate constants that validate this analysis, we simulated the wild-type data as we had for the mutant. Figure 4B illustrates wild-type data collected at 466 nm, using high and low (1.8 mM and 120 μM) substrate concentrations, overlaid with simulations obtained using the values for the rate constants given in Table 2. Again, though this set of values may not be the only solution that satisfactorily simulates the data, it is the only one discovered that faithfully reproduced all the data modeled. It is important to note that the value for k_5 is the *minimal* one that reproduces the data satisfactorily and also results in no detectable amount of CT absorbance, assuming the ϵ_{CT} is equal to that determined for the mutant and the detection limit in the stopped-flow apparatus is 0.002 absorbance unit.

Comparison of the simulated values for the wild-type and mutant enzymes in Table 2 suggests that the mutation has a much greater impact on this reaction than is suggested by comparison of the observed rate constants. From the maximal k_{obs} for reoxidation of the wild type (56 s^{-1}) and the maximal

k_{2obs} in the mutant (1.55 s^{-1}), it appears that the mutation results in a decrease of only 35-fold. However, a direct comparison of k_5 obtained in the simulations indicates a decrease of at least 440-fold in the rate for electron transfer. Since the estimated value for k_5 in the wild type is just a minimum, the real effect of the mutation may be much greater. In addition to this major effect, the simulations also suggest that the mutation decreases the affinity of the enzyme for hexenal in the initial Michaelis complex about 3-fold, and increases the rate constant for conversion of the Michaelis complex to the CT intermediate about 2-fold. The opposite direction of these effects suggests that the tyrosyl hydroxyl group may participate directly or indirectly (via water molecules) in a hydrogen bonding interaction with the carbonyl of the substrate to enhance binding in the wild-type Michaelis complex relative to that in the mutant, while at the same time slowing the transfer into the normal orientation for CT formation and reduction by the flavin.

Reaction Product Analysis. Given the different reactivities of the wild-type and Y206F enzymes, we wanted to confirm that the regiochemistry of reduction is preserved in the mutant. In separate experiments, a straight chain (*trans*-2-hexenal), a cyclic (2-cyclohexen-1-one), and an aromatic (cinnamaldehyde) substrate were incubated with NADPH and either the mutant or the wild-type protein. The GC retention times of the products using each substrate with either enzyme individually were consistent with the corresponding compounds in which the olefinic bond was reduced. No other products were detected (data not shown).

DISCUSSION

As described in the introduction, the Y206F mutation was introduced into EBP1 primarily to test the hypothesis that this highly conserved residue serves as an acid catalyst in the oxidative half-reaction. However, steady-state kinetic and inhibition data for EBP1(*3*) and the structures of OYE1 (*4*) indicate that both oxidizing and reducing substrates as well as phenoxide ligands for these enzymes bind in the same active site pocket between the flavin cofactor and this tyrosyl residue. Since the interactions of the substrates and ligands with the flavin are all of an electronic nature, it might be expected that the Y206F mutation, which removes a highly polar hydroxyl group presumably from the immediate vicinity of the substrate/ligand binding site, would exhibit effects beyond that associated with loss of an acid catalyst. Thus, in the studies presented here, we have examined the effects of the mutation on all three types of interactions: the binding of a phenoxide ligand, reduction by NADPH, and oxidation by hexenal. As mentioned above, during the course of our studies on EBP1, Kohli and Massey (*1*) reported effects of the same mutation (Y196F) on several properties of OYE1. Although some of the results are similar in the two proteins, there are also some salient differences that will be highlighted below.

In EBP1, the effects of the mutation on the binding of phenol are quite striking. Perhaps the most dramatic effect is the 30 nm red shift in the λ_{max} for the charge-transfer band of the phenoxide complex, which, at the wavelengths involved, corresponds to a decrease in the energy for the transition of 2.4−2.5 kcal/mol. Since CT transitions involve molecular orbitals from both the donor and acceptor, the decreased energy of the transition in the mutant could result from a decrease in the energy of the flavin acceptor orbital, an increase in the energy of the phenoxide donor orbital, or a combination of changes in both orbitals. It has previously been shown for OYE that changes in the midpoint potential for the flavin give a reasonably good measure of the change in energy of the flavin acceptor orbital in CT transitions. Thus, when modified flavins of variable midpoint potential are incorporated into OYE, a linear correlation is found between the midpoint potentials and the energy of the CT transitions with a given phenoxide ligand; the slope of the correlation is approximately 1.0−1.5 kcal/mol change in the energy of the CT transition for every kilocalorie per mole change in the redox equilibrium (*2*, *17*). Assuming a similar correlation for EBP1, the 13 mV increase in the reduction potential measured for the Y206F mutant relative to wild type suggests the energy of the flavin acceptor orbital is decreased by 0.6−0.9 kcal/mol, accounting for only part of the 2.4−2.5 kcal/mol decrease in the CT transition energy. Thus, it appears that the energy of the negatively charged phenoxide donor orbital is also increased in the mutant complex by as much as 1.5−1.8 kcal/mol. The higher energy could result from the lower local dielectric in the absence of the tyrosyl hydroxyl group. A similar effect on a CT donor orbital has been observed in mercuric ion reductase, where the energy of the CT transition between the active site cysteine thiolate and FAD was substantially lowered by mutation of the neighboring cysteine to the aliphatic residue, alanine (*18*). In that case, the reduction potential of the flavin was only minimally affected by the mutation, indicating that the decrease in energy of the CT transition must be solely attributed to an increase in the energy of the negatively charged thiolate donor orbital in the more hydrophobic active site.

Concomitant with the shift in energy of the CT transition, the pH profile indicates a further lowering of the pK_a for bound phenol and an enhanced affinity of the mutant for the ligand ranging from 2-fold at low pH to a maximum of 35-fold over that of wild type at high pH. A 5-fold enhancement of affinity at high pH can be attributed to the elimination of a repulsive electrostatic interaction between the tyrosine anion and the phenoxide anion. This is demonstrated by the loss of the tyrosyl hydroxyl pK_a of 8.7 that is perturbed to 9.4 in the pH profile for binding of phenoxide to the wild-type enzyme. The 2-fold effect at low pH and the additional 7-fold enhancement at high pH should then reflect an amplification of both the electronic interaction between the ligand and the flavin, and hydrogen bonding interactions between the phenoxide oxygen and groups in the active site. On the basis of the OYE1 structure, the ligand should form two hydrogen bonds with the His/His pair that is homologous with the His/Asn pair in OYE1. A strengthening of these interactions would occur with the increase in the negative charge density localized on the phenoxide oxygen, as expected for the increased hydrophobicity at the aromatic ring of the ligand created by the Tyr → Phe mutation. Furthermore, it is likely that concentration of electron density on the oxygen would lead to a stronger electronic interaction with the flavin, since the oxygen is positioned directly above the N1−O2α region of the flavin that lies within hydrogen bonding distance of a conserved, positively charged Arg. Thus, the enhanced affinity in the mutant is consistent with an elevation of the energy of the

donor orbital, as mentioned above.

The effects of the Y206F mutation on phenol binding to EBP1 are undoubtedly the most disparate from those observed in OYE1. In contrast to the dramatic red shift of the phenoxide CT band, blue shifts were observed in the CT bands of four different phenolic complexes of the OYE1·Y196F mutant, indicating an increase rather than a decrease in the energy of the CT transitions (*1*). The surprisingly opposite effect of this mutation in the two proteins highlights the need for caution in making predictions for one protein based only on the structure of a homologue, and focuses attention on identifying residues within the environment of the flavin and binding pocket of OYE1 that are not conserved in the aligned sequence of EBP1. Comparison of the sequences indicates that all of the residues forming hydrogen bonds to the flavin (R243, Q114, and T37 in OYE1) are conserved, as is the tyrosine of interest (Y196 in OYE1[2]) and its neighboring tryptophan (W116 in OYE1) whose position suggests it is the major factor lowering the tyrosine pK_a.[3] However, there are differences in residues both above and below the isoalloxazine ring of the flavin that may be expected to alter the flavin redox properties or the positioning of the ligands in the binding site. In OYE1, the residues packed behind the isoalloxazine ring (IPPL) form a solid hydrophobic backdrop with a low dielectric constant. In contrast, the sequence in EBP1 (YVPT) suggests the region in this protein has a much higher dielectric constant and perhaps a distinct dipole if the Y and T hydroxyls are held in a rigid hydrogen bonding interaction. This may be the main reason for the lower midpoint potential (16 mV) in wild-type EBP1(*3*) versus wild-type OYE1, and, likewise, may contribute to the opposite effects of the Y206F and Y196F mutations on the flavin potentials in the two proteins. The other obvious sequence difference occurs in the residues of the loop that binds the active site ligands. In OYE1, the binding residues are a His/Asn pair in the sequence HSAN, while in EBP1, the residues are a His/His pair in the sequence HGAH. Although the second histidine can be modeled to position its δ-nitrogen in the same position as the asparagine nitrogen, the alternative conformations of a histidine provide more flexibility in positioning the ligands, especially in their orientation with the tyrosine residue mutated in these studies. In addition, the side-chain hydroxyl of serine in the OYE1 loop is packed into a hydrophobic pocket so that it forms a strong hydrogen bond with its own backbone carbonyl oxygen, which should significantly stabilize the conformation of the loop and the positioning of the His/Asn pair. The replacement of this serine by a glycine in EBP1, however, would be expected to decrease the rigidity of the loop itself, thereby allowing additional flexibility in positioning the His/His pair and, hence, the ligands bound to them in the active site. The sum of these differences in the positioning of the ligands relative to the tyrosines within the active sites of the two proteins could account for the opposite impact of the mutation on the energies of these bound ligands. The previous observation that nortestosterone can undergo both oxidation and reduction in the active site of EBP1 (*3*), but only reduction in the active site of OYE1 (*19*), supports this hypothesis.

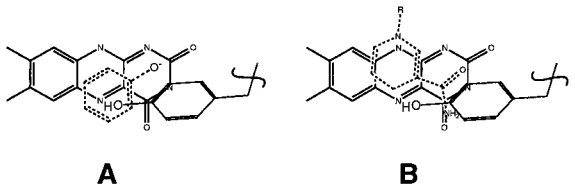

FIGURE 5: Proposed orientation of phenoxide and NADPH in the EBP1 active site. Positions of phenoxide (A) and NADPH (B) were rendered in CS ChemDraw Pro, based on the analogous crystal structures of OYE1 and kinetic data for EBP1 that indicate reduction of the flavin occurs via transfer of the *pro-R* hydride from NADPH.

The proposal that Tyr206 serves as a general acid catalyst in the second half-reaction implies that the effect of its mutation on the first half-reaction should be minimal since no proton transfers are required in this reaction. This is borne out in the data, where the mechanism for this half-reaction appears to be unaffected, and there are only small differences in the microscopic kinetic constants. Of interest, the results indicate that the equilibrium governing the flavin reduction is smaller than expected from the 13 mV decrease in the midpoint potential ($k_5/k_6 \approx 0.15$ versus 0.28 expected). This is consistent with the observation that, unlike the phenoxide CT band, no significant shift occurs in the CT band for the mutant complex with NADPH (data not shown), suggesting either that the mutation has a minimal effect on the flavin and NADPH orbitals in this complex or that it causes a similar decrease in the energies of both orbitals. The much smaller impact of the mutation on NADPH vs phenoxide may result in part from its lack of a negative charge. However, as illustrated in Figure 5, a difference in the position of the NADPH ligand relative to the tyrosyl hydroxyl group could also play a role. This orientation of NADPH, which is required by the *pro-R* stereochemistry of the hydrogen transfer from NADPH to the flavin (Buckman and Miller, *21*), suggests the CT donor orbital (the delocalized electrons from the nicotinamide nitrogen) is further removed from the tyrosyl hydroxyl than occurs with the phenoxide ligands and therefore less influenced by the mutation. Similar results were reported for this reaction in the OYE1·Y196F mutant (*1*).

In contrast to the minimal changes in the reductive half-reaction, the oxidative half-reaction is very different in the wild-type and Y206F mutant proteins. The most obvious difference is the generation of a novel intermediate in the reaction and the concurrent switch from monophasic to biphasic kinetics. In the reaction of HXL with wild type, there is apparently no generation of the CT intermediate. As discussed above, this is consistent with the same mechanism acting in the two proteins (Scheme 3), where the relative values of k_3, k_4, and k_5 are such that the intermediate does not accumulate in wild type, $k_5 \gg k_3 + k_4$. If the value of $k_3 + k_4$ becomes significant with respect to k_5, more of the intermediate is formed, and when $k_3 + k_4$ is very much larger than k_5, as occurs in the mutant, equilibrium formation of the CT species is complete before

[2] Although the pH dependence was not reported for binding of phenols to the Y196F mutant of OYE1 (*1*), we would predict from our results that the pK_a of 8.4 previously observed in the pH profiles for wild-type OYE (*2*) is due to Y196 and, hence, should be missing from a pH profile for the mutant.

[3] The structure of the *p*-hydroxybenzaldehyde·OYE1 complex reveals that the indolyl N−H bond points directly at the benzyl ring of Y196, suggesting the donation of a hydrogen bond from W116 that would substantially stabilize the delocalization of electrons from the deprotonated tyrosyl hydroxide into the ring, lowering its pK_a.

oxidation proceeds. While we cannot rigorously exclude the possibility that the wild-type mechanism is different, it is difficult to imagine how the mutation would allow formation of such a catalytically activated species poised for reaction (*20*) if it does not form in the wild-type enzyme.

The stabilization of the reduced enzyme·substrate CT complex in the mutant protein argues strongly that Y206 does act as a proton donor to facilitate the oxidative half-reaction. However, the failure to completely abolish reduction of the substrate raises the question of whether Y206 is truly an obligatory acid catalyst. It is important to note that the studies described here were conducted with what is most likely an artificial substrate, and, thus, the architecture of the active site is not optimized for it. Perhaps the residual activity results from exposure of the reactive intermediate to solvent, from which it can abstract a proton. In contrast, a compound better able to exclude solvent from the active site would be more dependent on the acid catalyst. Studies with the homologous mutant of OYE1 may lend support to this idea: the ability to reduce the three compounds tested in the absence of the catalytic tyrosine was found to be highly dependent on the structure of the substrate (*1*). Another possible explanation is that the mutant is able to utilize an alternative, albeit energetically less favorable, reaction path. For instance, if His204 in EBP1, analogous to Asn194 that hydrogen bonds to the substrate carbonyl oxygen in OYE1, is also hydrogen bonded to a water molecule at its other nitrogen, it may provide a path for protonation of the substrate oxygen to form an enol product. Nevertheless, the substantial effect of the mutation on reduction of this compound attests to its importance in this half-reaction. The conservation of this residue, not only among other members of the OYE family but also in EBP1, implies that the relevant reactions catalyzed in vivo cannot proceed at the required rate without it.

In summary, one of the primary goals of this work was to develop an enzyme that maintains the ability of the wild-type protein to bind the physiologically relevant substrate, but is unable to significantly reduce that compound. It is difficult to predict without any knowledge of the true nature of the substrate how the mutation will alter the interaction between it and the protein. Still, the enzyme described here does exhibit the desired properties, and experiments are underway to characterize the physiological electron acceptor of this enzyme using this mutant.

ACKNOWLEDGMENT

We thank Laura Koo and Dr. John Cantwell for technical advice in the operation of the GC and FPLC systems, respectively.

REFERENCES

1. Kohli, R. M., and Massey, V. (1998) *J. Biol. Chem. 273*, 32763−32770.
2. Abramovitz, A. S., and Massey, V. (1976) *J. Biol. Chem. 251*, 5327−5336.
3. Buckman, J., and Miller, S. M. (1998) *Biochemistry 37*, 14326−14336.
4. Fox, K. M., and Karplus, P. A. (1994) *Structure 2*, 1089−1105.
5. Chen, H. Y., Demidkina, T. V., and Phillips, R. S. (1995) *Biochemistry 34*, 12276−12283.
6. Xue, L. A., Talalay, P., and Mildvan, A. S. (1990) *Biochemistry 29*, 7491−7500.
7. Ellis, K. J., and Morrison, J. F. (1982) *Methods Enzymol. 87*, 405−426.
8. Dixon, M. (1953) *Biochem. J. 55*, 161−170.
9. Strickland, S., Palmer, G., and Massey, V. (1975) *J. Biol. Chem. 250*, 4048−4052.
10. Matthews, R. G., Massey, V., and Sweeley, C. (1975) *J. Biol. Chem. 250*, 9294−9298.
11. Krishnan, A. V., Stathis, P., Permuth, S. F., Tokes, L., and Feldman, D. (1993) *Endocrinology 132*, 2279−2286.
12. Powell, B. L., Frey, C. L., and Drutz, D. J. (1984) *Exp. Mycol. 8*, 304−313.
13. Skowronski, R., and Feldman, D. (1989) *Endocrinology 124*, 1965−1972.
14. Porter, D. J., and Bright, H. J. (1980) *J. Biol. Chem. 255*, 7362−7370.
15. Dawson, R. M. C., Elliot, D. C., Elliot, W. H., and Jones, K. M. (1969) in *Data for Biochemical Research*, Clarendon Press, New York.
16. Gorelick, R. J., Schopfer, L. M., Ballou, D. P., Massey, V., and Thorpe, C. (1985) *Biochemistry 24*, 6830−6839.
17. Stewart, R. C., and Massey, V. (1985) *J. Biol. Chem. 260*, 13639−13647.
18. Distefano, M. D., Au, K. G., and Walsh, C. T. (1989) *Biochemistry 28*, 1168−1183.
19. Vaz, A. D. N., Chakraborty, S., and Massey, V. (1995) *Biochemistry 34*, 4246−4256.
20. Massey, V., and Ghisla, S. (1974) *Ann. N.Y. Acad. Sci.*, 446−465.
21. Buckman, J., and Miller, S. M. (2000) *Biochemistry 39*, 10521−10531.
22. Djordjevic, S., Dong, Y., Paschke, R., Frerman, F. E., Strauss, A. W., and Kim, J. J. (1994) *Biochemistry 33*, 4258−4264.
23. Ghisla, S., Thorpe, C., and Massey, V. (1984) *Biochemistry 23*, 3154−3161.

BI000653S